Final Measurement and Verification Report for I&T Trial Project

Combination of 3D Printing Technology and Reverse Engineering for Making Critical Spare Parts of Complex Systems

I&T Project No. : P-0005
I&T Wish No. : W-0085
I&T Solution No. : S-0012

E&M InnoPortal

EMSD

Copyright Notice And Disclaimer

Copyright Notice

Disclaimer

Table of Contents

Purpose of the Project and Target Deliverables

EMSD has commissioned the Department of Mechanical Engineering the Hong Kong Polytechnic University to carry out a comprehensive study on the technology for fabrication of the critical parts for maintenance and emergency repair aided by 3D modelling, Reserve Engineering (RE) and simulation technologies, from 8 January 2018 to 7 July 2019.

They shall provide the following items to facilitate maintenance at the trial venue,

(i) 3D printed part of a metal alloy cube

(ii) 3D printed part of an engineering plastic worm gear

Project Description

In this project, a target system for shooting used by the Hong Kong Police Force has been taken as a study case, as shown in Fig. 1. The gear box in the shooting system contains two critical parts, a cube and a worm gear, which were originally made of aluminum ally and plastics, respectively. RE combined with 3D Printing technology was applied as a method to fabricate and re-design the cube and worm gear with optimized material selection and part geometry design. Up to now, the cube and the worm gear have been fabricated by combing RE and 3D printing technology with selected materials, and illustrate good geometrical accuracy and better mechanical properties than the original ones, thus can be good candidates applied in the target shooting system

Fig. 1 The shooting system: (a) shooting range, (b) and (c) control unit and (d) gear

Trial Site

The trial site is at the Hong Kong Police Force shooting system venue.

Type of Equipment/ Installation/ Technology Adopted

Reverse Engineering (RE) / Generation of 3D Model

Based on RE technology, the process starts with utilizing an optical 3D scanner efficiently and accurately for scanning the parts and creating point clouds. The 3D scanner software allows the direct conversion of the aligned scans (i.e., the cumulative point clouds) in a 3D polygon mesh (usually in STL format), which is then imported into the CAD software SolidWorks for modifying and reconstruction of the geometry of the parts. Finally, the optimized 3D CAD model is exported in polygon mesh format which is required for 3D printing.

3D Printing

With the selected materials, the cube and worm gear are printed by dedicated 3D printers with different printing technologies (i.e. MJF and FDM). The selected materials and corresponding 3D printers are detailed in "Methodology and Applicable Standards" section.

Evaluation of 3D printing parts

Mechanical properties of 3D printing parts are evaluated by comparing with those of original parts. Besides, GOM Inspect Software is used to evaluate the geometry and dimension of 3D printing parts by comparing the 3D measurement data derived from 3D scanner with the CAD data. As a result, problematic areas of parts can be identified intuitively in a colored deviation plot given by the software.

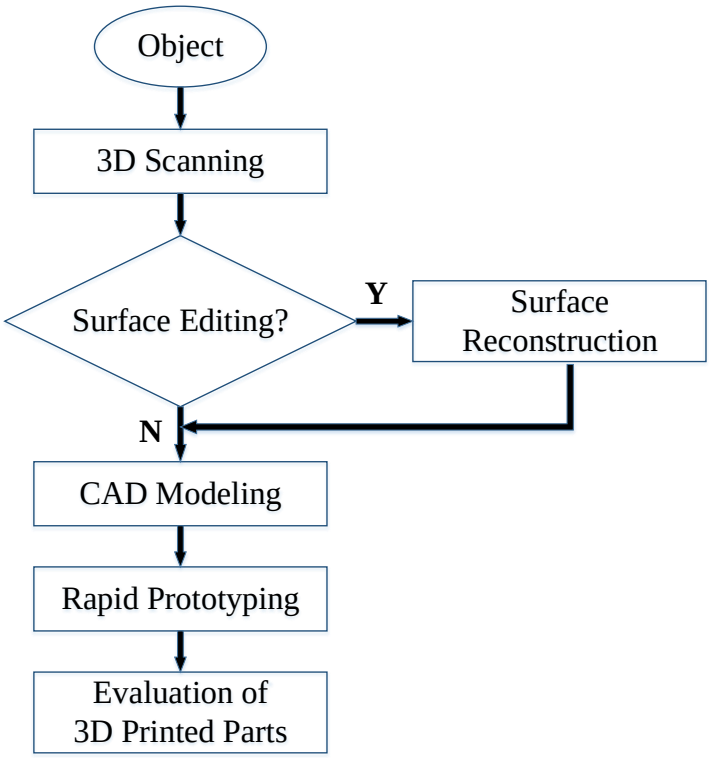

Fig. 2 Research Procedure

Trial Timeframe

From 8 January 2018 to 7 July 2019, the trial is conducted.

Name and Background of I&T Solution Provider

The Department of Mechanical Engineering in the Hong Kong Polytechnic University collaborated with EMSD in this project. The department aims to achieve excellence in education and research in the discipline of mechanical engineering with global out-reach and impact.

Details of Implemented Trials

I. Methodology and Applicable Standards

(i) Metal Alloy Cube

(1) 3D scanner

ATOS Core 200, an optical 3D scanner based on fringe projection, was used to deliver accurate and traceable 3D coordinates of the cube for 3D printing, as shown in Fig. 3.

Fig. 3 The 3D scanner ATOS Core 200

(2) Material and 3D printer

For printing the cube, stainless steel 316L powder was selected as a substitute of aluminum because of its excellent strength and wear resistance, making it a good candidate for durable prototypes and spare parts. The cube was printed by a Selective Laser Melting (SLM) 3D printer SLM280 2.0 (Twin 400Wx2) made in Germany, as shown in Fig. 4(a). Specifically, SLM is a particularly 3D printing technique designed to use a high power-density laser to selectively melt and fuse metallic powders together, layer by layer until the part is complete. SLM can produce strong, durable metal parts that work well as both functional prototypes or end-use production parts. In addition, to evaluate the forming quality of 3D printer SLM280, comparative experiments of 3D printing part in stainless steel 316L powder were carried out using a SLM based 3D printer WXL-120 made in mainland China, as shown in Fig 4(b).

Fig. 4 The 3D printers for printing the cube: (a) SLM280 and (b) WXL-120

(ii) Engineering Plastic Worm Gear

(1) 3D scanner

ATOS Core 200 mentioned in Fig. 3 was also used to scan the worm gear for further process.

(2) Materials and 3D printers

To print the worm gear, two thermoplastics, viz. ABSplus-P430 and PA 12 (i.e. Nylon 12), were selected as candidate materials for making the worm gear for their good wear resistance and widespread applications on durable prototypes and end-use-parts. Two 3D printing technologies, viz. Fused Deposition Modeling (FDM) and Multi Jet Fusion (MJF), were used to print the worm gear with the materials mentioned above.

FDM is a filament-based technology where a temperature-controlled head extrudes a thermoplastic material layer by layer onto a build platform. A support structure is created where needed and built in a water-soluble material. The great advantage of FDM is the durable materials it uses, the stability of their mechanical properties over time, and the quality of the parts. In this project, two 3D printers with FDM technology were used to print the worm gear, with ABSplus-P430 printed on FDM uPrint SE plus and Nylon 12 on FDM Fortus 900MC, as shown in Fig. 5 (a) and (b).

MJF is a powder-based technology but does not use laser. The powder bed is heated uniformly at the outset. A fusing agent is jetted where particles need to be selectively molten, and a detailing agent is jetted around the contours to improve part resolution. While lamps pass over the surface of the powder bed, the jetted material captures the heat and helps distribute it evenly. MJF uses fine-grained PA 12 powder that allows for ultra-thin layers of 80 microns, resulting in the high density and low porosity of the produced parts. It can also produce exceptionally smooth surfaces straight out of the printer, and the functional parts need minimal post-production finishing. In this project, the 3D printer MJF 4200/3200 was used to print the worm gear with PA 12 powder, as shown in Fig. 5 (c).

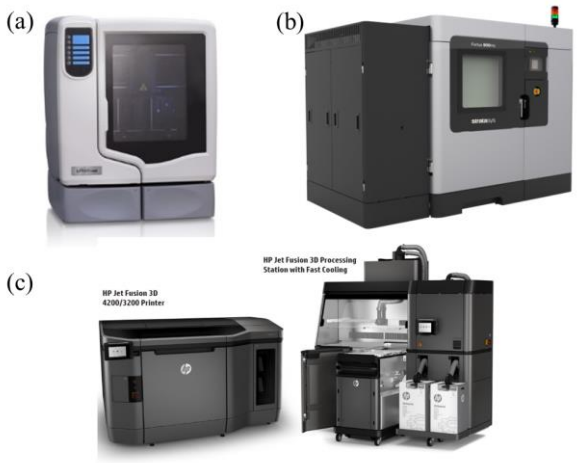

Fig. 5 The 3D printers for printing the worm gear:

(a) FDM uPrint SE plus,

(b) FDM Fortus 900MC and

(c) MJF 4200/3200

II. Measurement and Verification Activity Details

Facilities for evaluation

(i) Metal Alloy Cube

To investigate mechanical properties (tensile property and hardness) of both the original and fabricated cubes, tensile tests were conducted on MTS Alliance RT/50 (maximum load: 50kN) and hardness tests were carried out on a full-automatic hardness tester LC-200RB. Furthermore, to evaluate the microstructures of the 3D printing parts, Scanning Electron Microscope (SEM) observations of polished surface and fractured surface of tensile specimens were conducted on VEGA3 TESCAN.

(ii) Engineering Plastic Worm Gear

To compare the mechanical properties of both the original and fabricated parts, tensile tests were conducted on the tensile test instrument Instron Electropuls E10000 (maximum load: 10kN).

Summary Results and Analysis

I. Pre and Post-installation Comparison

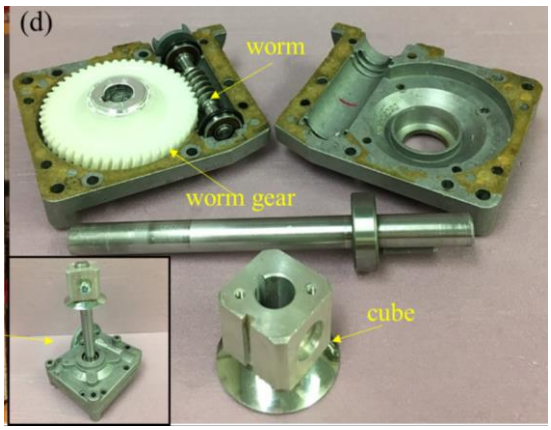

The 3D printed parts shall act as a spare part for the shooting practice system (cube and worm gear in the above mechanical system).

II. Key Statistics/ Figures/ Infographics to Support the Results

(i) Metal Alloy Cube

Table 1 Print settings of the cube on SLM 280

Machine	SLM280 2.0 (Twin 400W x 2)
Laser power used	200W
Energy density	70 J/mm³
Build Time	around 6 hrs per block (not incl. post-processing)
Materials used	stainless steel 316L
Particle size distribution	10 - 45 µm
Grain shape	Spherical
Layer thickness	30 µm

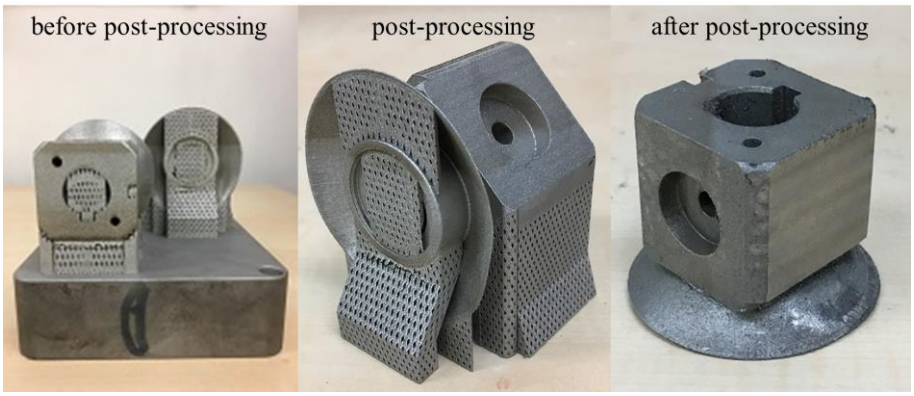

Fig. 7 The 3D printed cube on SLM 280

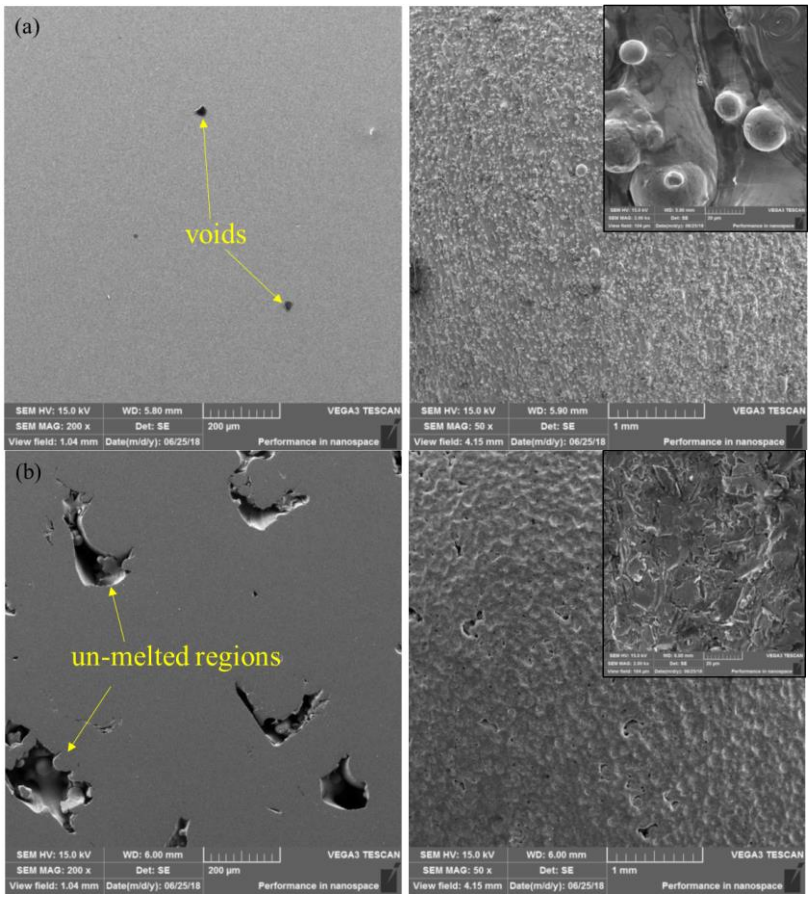

Fig. 8 SEM micrographs of the polished surface (left column) and the as-printed surface (right column) of the workpieces printed by: (a) SLM280 and (b) WXL-12

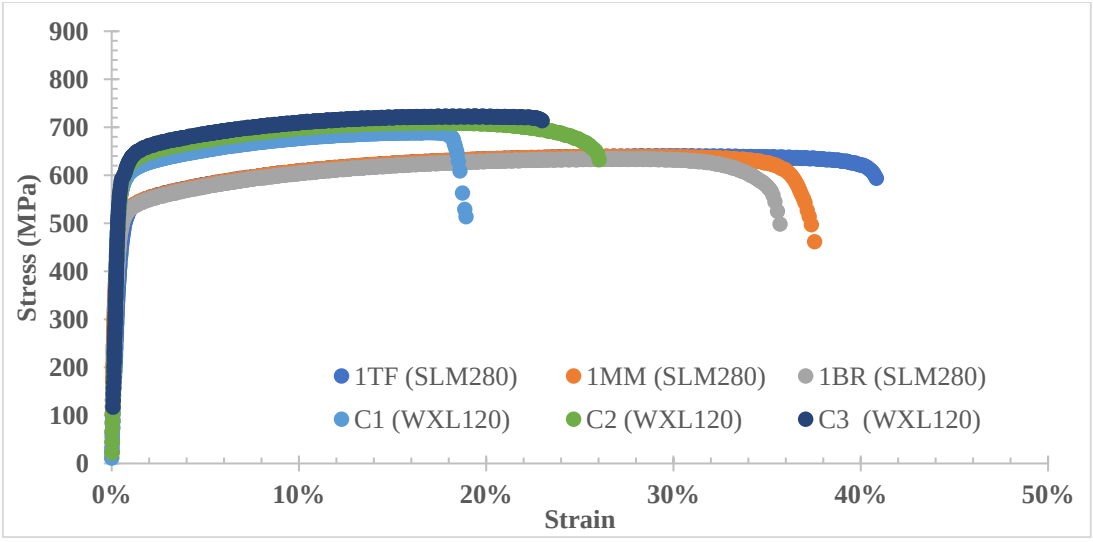

Fig. 10 Strain-stress curves of 316L specimens printed by SLM 280 and WXL-120

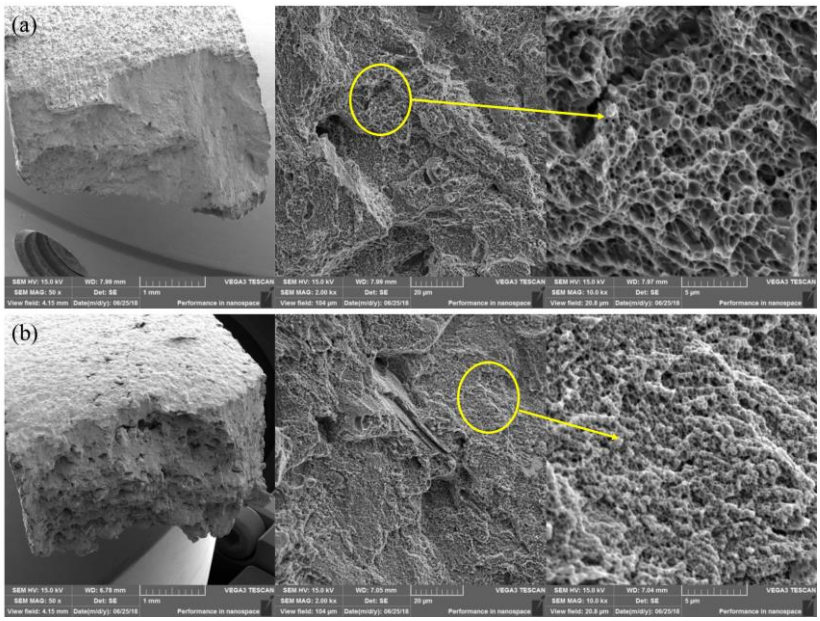

Fig.11 SEM images of fracture surfaces of specimens printed by:
(a) SLM 280 and (b) WXL-120

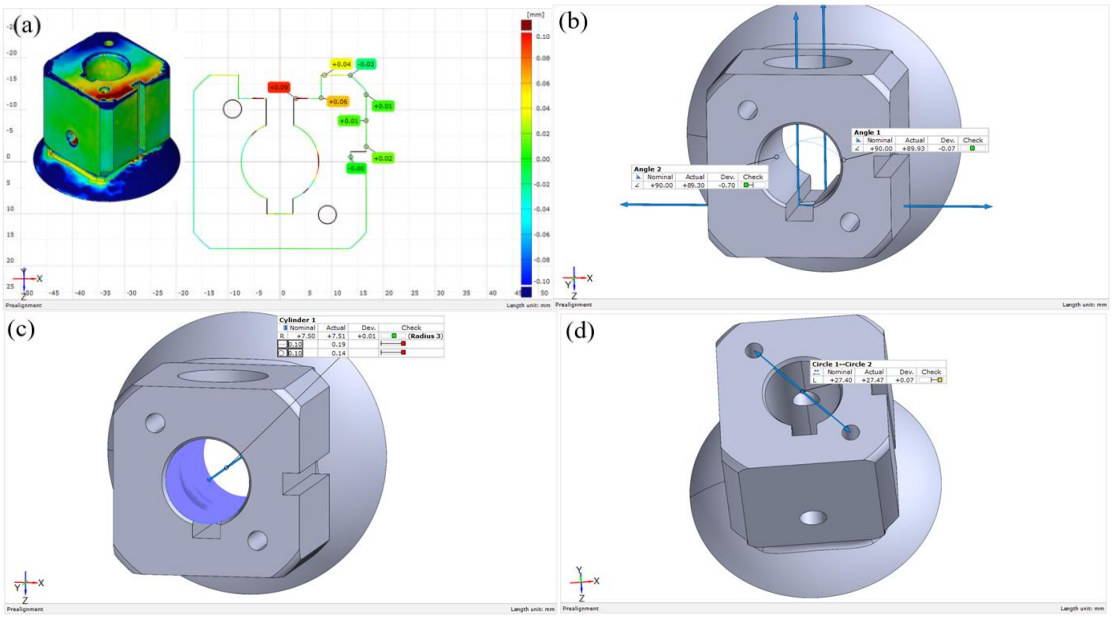

Fig. 13 Deviation plot of the cube: (a) Z-axis cross section, (b) angles,
(c) radius/diameter and (d) center to center

(ii) Engineering Plastic Worm Gear

Table 3 Printing settings of PA 12 worm gear

Mass of Worm Gears	840 g / 12 pcs
Processing Height	30.5 mm
Processing Time	2h 43m
Fusing Agent Usage	88 cc
Detailing Agent Usage	125.6 cc
Building Mode	Cosmetic

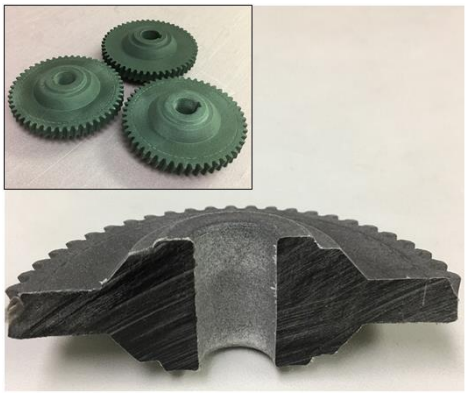

Fig. 17 3D printed worm gear of PA 12

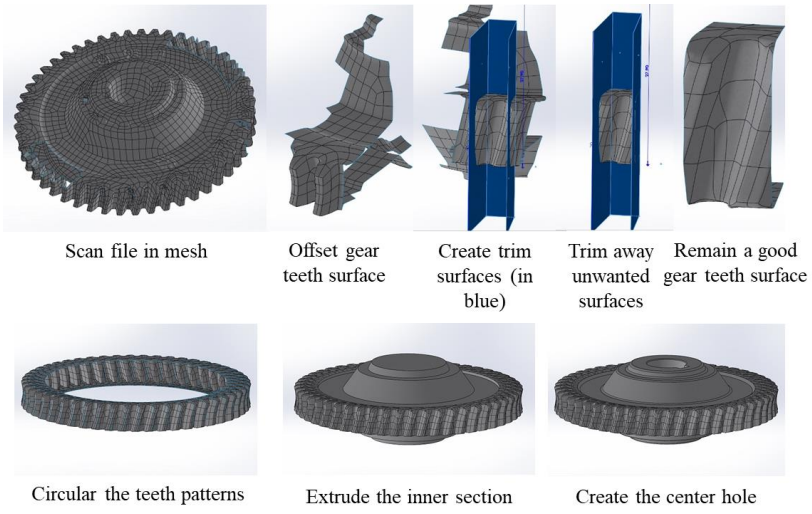

Fig. 15 3D surface reconstruction of the worm gear

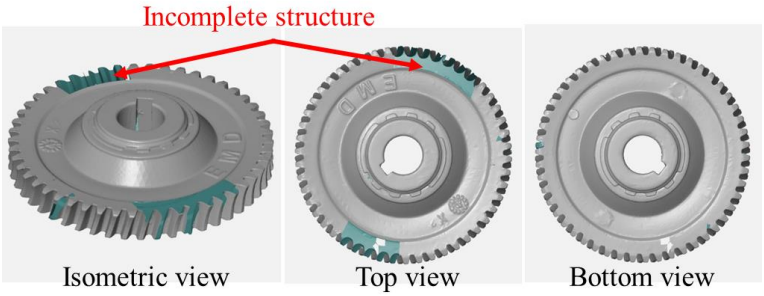

Fig. 14 3D scanned model of the original worm gear

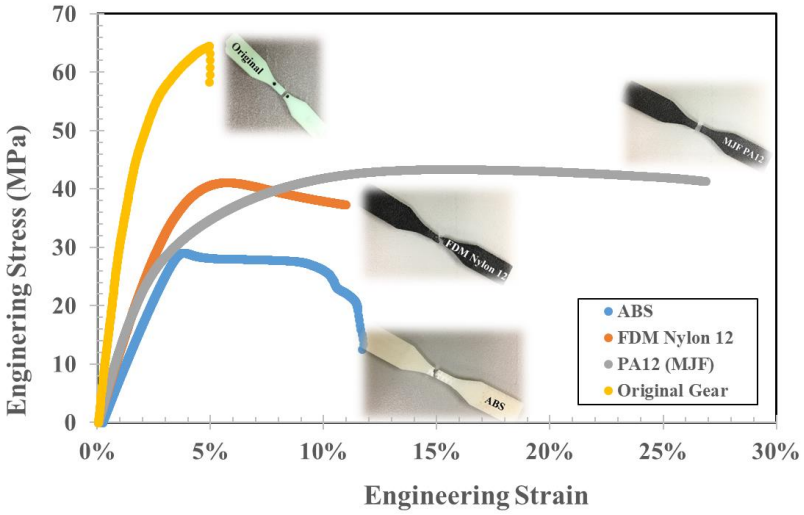

Fig. 19 Engineering strain-stress curves of the original gear and 3D printed gears using ABS, Nylon 12 (FDM) and PA 12 (MJF)

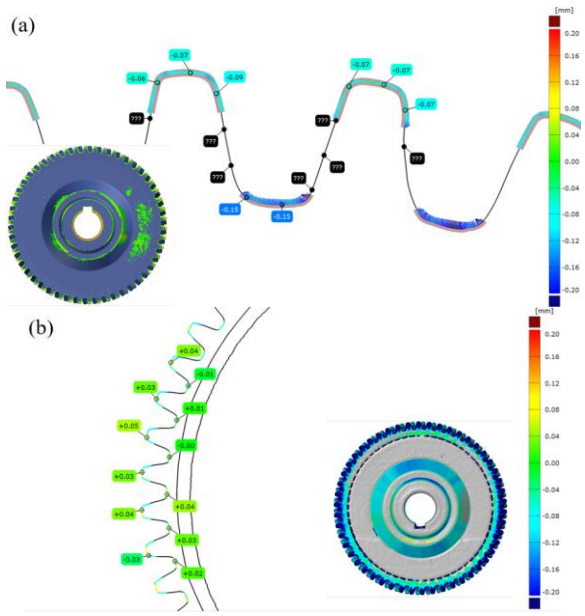

Fig. 20 Z-axis cross section inspection of worm gear:
(a) The first printed sample and (b) The second printed sample

III. Analysis of M&V Results to Address the Target Deliverables

(i) Metal Alloy Cube

3D model generation of the cube

Due to the comparatively simple geometry of the cube, we accurately measured the dimension of the original cube and created 3D model by 3D software Solidworks. Then the CAD file was exported in polygon mesh format (STL) for 3D printing. Fig. 6 shows the generated 3D model of the cube.

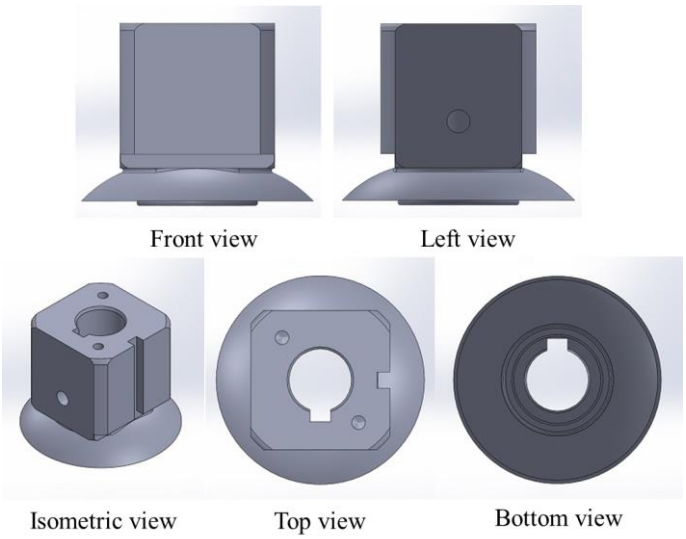

Fig. 6 The 3D CAD model of the cube

3D printing of the cube

As mentioned above, the 3D printer SLM280 was adopted to print the cube, and stainless steel 316L powder was selected as the replaced material, with spherical grain shape and 10~45um of particle size. Table 1 shows the print settings of the cube. After printing, post-processing was carried out including cutting down the support material. The 3D printing cube on SLM 280 is shown in Fig. 7.

Table 1 Print settings of the cube on SLM 280

Machine	SLM280 2.0 (Twin 400W x 2)
Laser power used	200W
Energy density	70 J/mm³
Build Time	around 6 hrs per block (not incl. post-processing)
Materials used	stainless steel 316L
Particle size distribution	10 - 45 μm
Grain shape	Spherical
Layer thickness	30 μm

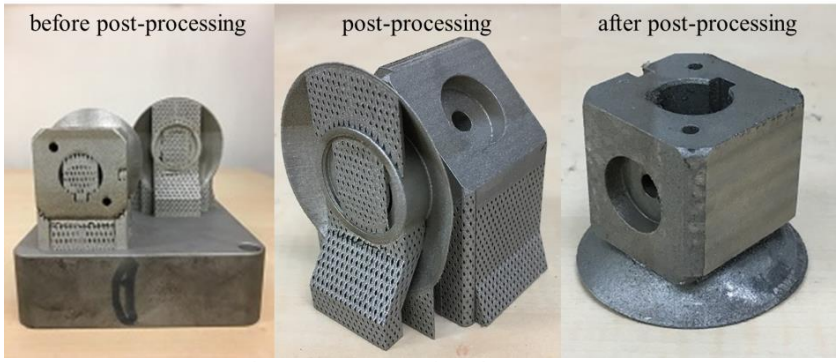

Fig. 7 The 3D printed cube on SLM 280

To evaluate forming quality of 3D printing parts by SLM280, including surface quality and mechanical property, the SLM based 3D printer WXL-120 was adopted for comparative experiment and study. Since microstructural features of the parts can influence the mechanical properties, such as defamation behavior and fatigue resistance, SEM observation of 3D printing specimens printed by the two printers were conducted to evaluate the microstructures. Fig. 8 shows the SEM micrographs of polished surface (left column) and the printed surfaces (right column) of specimens printed by the two 3D printers mentioned. Small and few spherical micro voids with an approximate size of 40μm are observed in the polished surface of specimen printed by SLM280 (left column of Fig. 8(a)). In contrast, many big irregular un-melted regions can be seen in that printed workpiece by WXL-120, reaching over 200μm (left column of Fig. 8(b)), and it is believed that such irregular defects could also exist inside the printed parts. The irregular pores in the microstructure are generated due to unstable molten pool or lack of complete melting, whereas the spherical pores in the microstructure are caused by trapped gas in melt pool. These microstructural defects, as a result, may have led to smaller elongation to failure and shorter fatigue life of the printed parts. It should be noted that

the more or the bigger the voids and the un-melted regions in the 3D printing parts, the more easily the parts could damage. Besides, the as-printed surface of the former illustrates higher density, with a layer of unfused particles adherent, which would not significantly affect the performance of the formed parts. However, many visible holes on the as-printed surface of the latter, which probably indicates low density of the specimen and could definitely result in bad mechanical property.

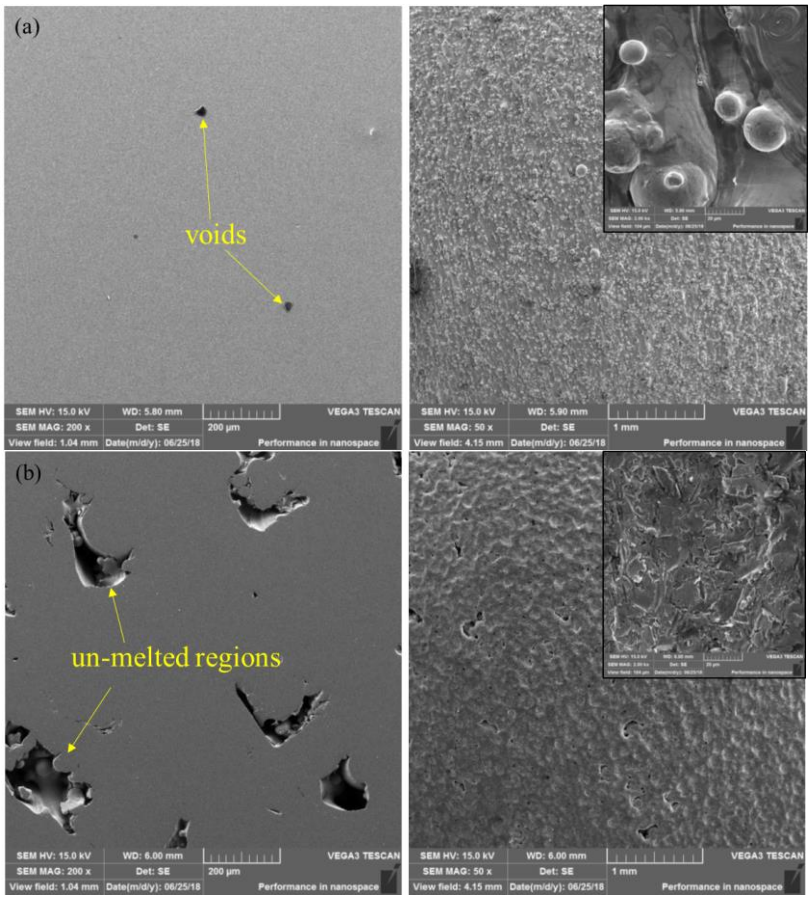

Fig. 8 SEM micrographs of the polished surface (left column) and the as-printed surface (right column) of the workpieces printed by: (a) SLM280 and (b) WXL-12

Mechanical property evaluation of 3D printed cube

To analyze the tensile property of the 3D printing cube, the tensile tests of 3D printing specimens in stainless steel 316L were conducted at room temperature on the tensile test instrument MTS Alliance RT/50, and SEM observations of the fracture surface were also implemented. These specimens for tensile tests were printed with the same settings as in printing the cube. The geometry of the specimen was designed according to the

standard ASTM E8-16a, as shown in Fig. 9. Before tests, these as print specimens needed to be polished to avoid defects on the surface.

For the specimens printed by SLM 280, to confirm whether the printing locations on the 3D printing substrate could influence the tensile property, three sites on the substrate were chosen to print tensile specimens, namely, in bottom right (BR), middle (MM) and top left (TF). Besides, three tensile specimens printed by WXL-120 were conducted for comparative study.

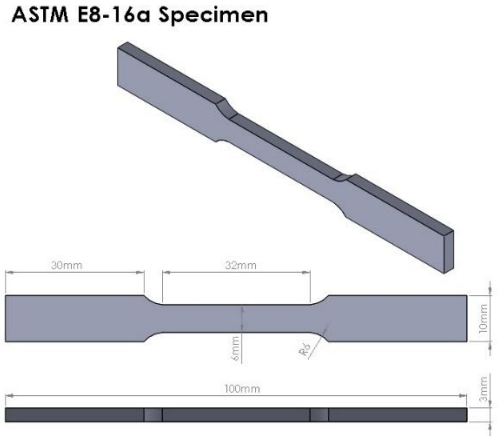

Fig. 9 ASTM E8-16a specimen

Fig. 10 shows the strain-stress curves of 316L specimens printed by SLM 280 and WXL-120. Different fracture elongations are obtained in different sites of SLM 280 printed specimens. The MM specimen printed in the middle site shows a medium fracture elongation of 37.5%, between that of the BR and TF specimens, 35.7% and 40.8%, respectively. Therefore, the TF site on the substrate could be a better selection for printing the cube for its higher fracture elongation. Furthermore, compared with those printed by WXL-120, SLM 280 printed specimens all enjoy higher fracture elongation, averagely 22.6% for the former and 38.0% for the latter. Such difference could be explained by the effect of microstructure mentioned in Section 4.2.

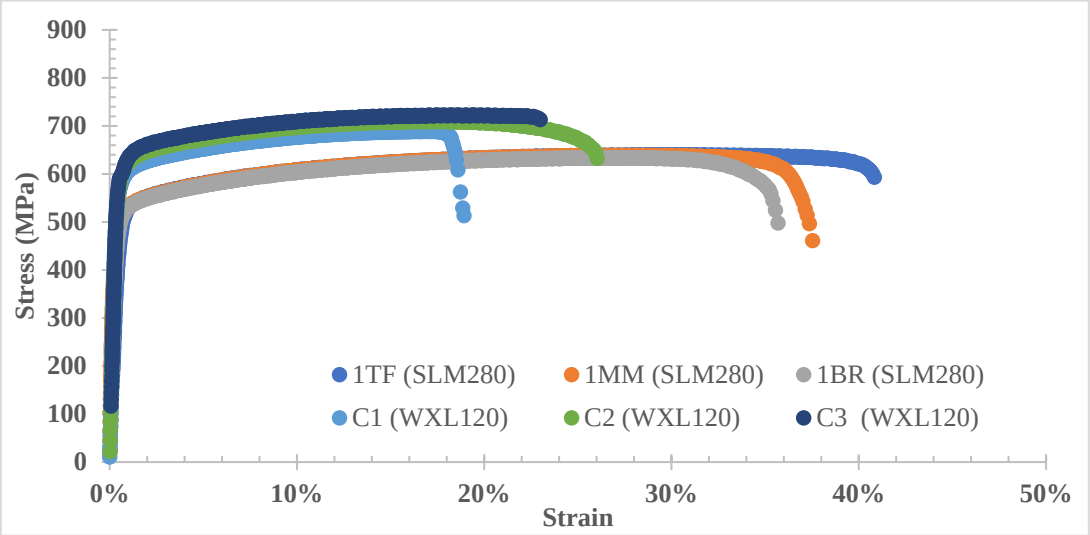

Fig. 10 Strain-stress curves of 316L specimens printed by SLM 280 and WXL-120

Fig. 11 illustrates SEM observations of fracture surfaces of specimens printed by SLM 280 and WXL-120. Many scattered small holes can be seen on the fracture surface of WXL-120 printed specimen (left column of Fig. 11(b)), while SLM 280 specimen shows a comparatively high density and low porosity, with few visible holes seen on fracture surface (left column of Fig. 11(a)). As mentioned in Section 4.2, the existence of fusion and/or trapped gas is the main reason for causing such defects, leading to the smaller elongation to fracture of the WXL-120 printed specimen. Besides, dimples, the main microscopic feature of metal plastic fracture, are observed on the fracture surface of both specimens, depicting a ductile fracture under tensile loading. It should be noted that the ductility of the alloy is proportionally to the size and depth of the dimples. Larger and deeper dimples observed on the fracture surface of SLM 280 printed specimen (right column of Fig. 11(a)), can explain the larger elongation to fracture and ductility, observed for this sample as compared to WXL-120 printed specimen. Since the specimens printed on SLM 280 demonstrate better performance, SLM 280 should be more suitable for printing the cube.

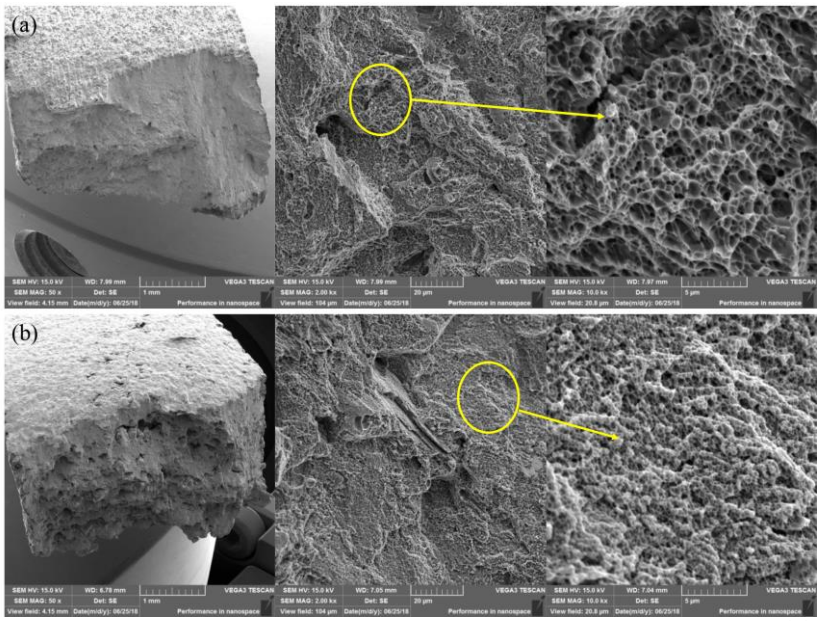

Fig.11 SEM images of fracture surfaces of specimens printed by: (a) SLM 280 and (b) WXL-120

Hardness tests were carried out to acquire the Vickers hardness of the original and 3D printed cubes (SLM 280) on the full-automatic hardness tester LC-200RB, with six measurements being obtained for each specimen to calculate the average value. The average hardness value is 90.4HV for the original aluminum cube and 301.6HV for the 3D printed cube by using stainless steel 316L, as shown in Table 2. Therefore, the 3D printed cube with 316L has a higher hardness and can serve as a good substitute for the original aluminum cube.

Table 2 Hardness of the original cube and 3D printed cube by SLM 280

Points	Original cube	3D printing cube
1	89.5	295.1
2	88.6	338.3
3	91.8	290.2
4	90.2	294.8
5	91.5	309.8
6	90.8	281.3
Average	90.4	301.6

Geometry analysis of 3D printed cube

To evaluate the forming accuracy of the 3D printing parts, they were firstly scanned by a 3D scanner. The 3D measurement data was then analyzed and verified by comparing with the CAD data using the software GOM

Inspect, in which 3D meshes of the parts were calculated from 3D point clouds for CAD comparison.

Fig. 12 shows the 3D scanning model of the 3D printing cube. The scanning file was imported into the software GOM Inspect for evaluation.

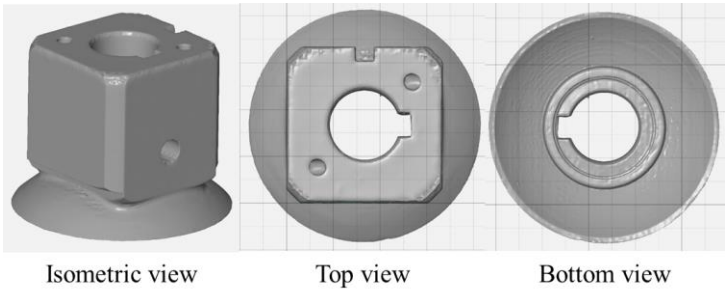

Fig. 12 The 3D scanned model of 3D printing cube

Fig. 13 is the deviation plot of the cube in terms of inspections of section, angle and radius/diameter. From the prealignment of the CAD and mesh bodies of the cube (Fig. 13(a)), the dimensional deviation ranges from -0.1 to +0.1mm. For the Z-axis cross section, the maximum deviation between mesh and CAD body is +0.09mm, which occurs mainly at the corner, while the majority remains comparatively low deviation. Meanwhile, the angle inspection, as well as radius/diameter and center to center inspection, also shows a low discrepancy. Thus, it can be concluded that the 3D printing cube has reasonable dimensional accuracy.

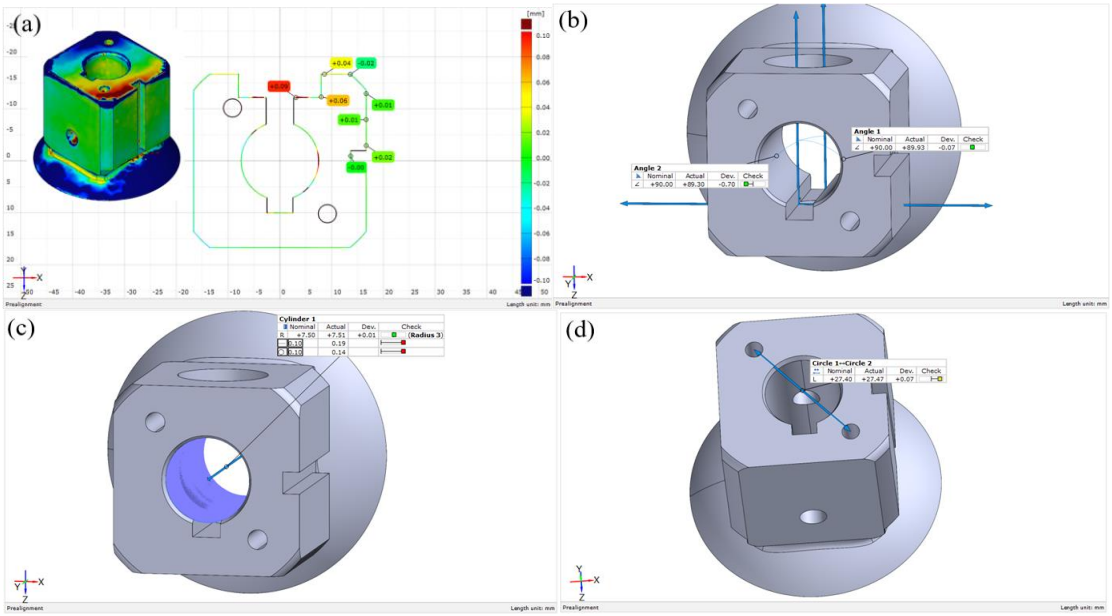

Fig. 13 Deviation plot of the cube: (a) Z-axis cross section, (b) angles,

(c) radius/diameter and (d) center to center

(ii) Engineering Plastic Worm Gear

3D model generation of the worm gear

The complex structure of the gear teeth on the worm gear makes it difficult to create 3D model by Solidworks directly. With the 3D scanning technology, the 3D scanner ATOS Core 200 can provide quick 3D acquisition from the original worm gear for in-house 3D printing. Before scanning, the worm gear was sprayed with white paint to avoid reflection, thus to be accurately captured by the camera. The scanned model of the original worm gear is shown in Fig. 14. It can be seen that the scanned model has some inevitable incomplete structures due to high complexity of the gear teeth. Necessarily, surface reconstruction was carried out to complete the model generation using Solidworks, as shown in Fig. 15. Based on the scanned file in mesh, a trim surface was picked out with unwanted surfaces removed and a good gear teeth surface remained. Then, we rotated the teeth patterns and extruded the inner section, with the center hole finally being created.

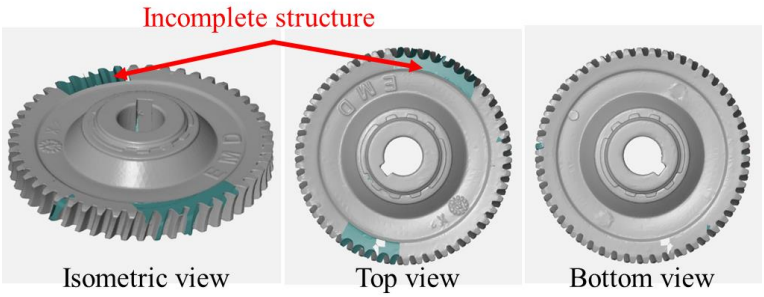

Fig. 14 3D scanned model of the original worm gear

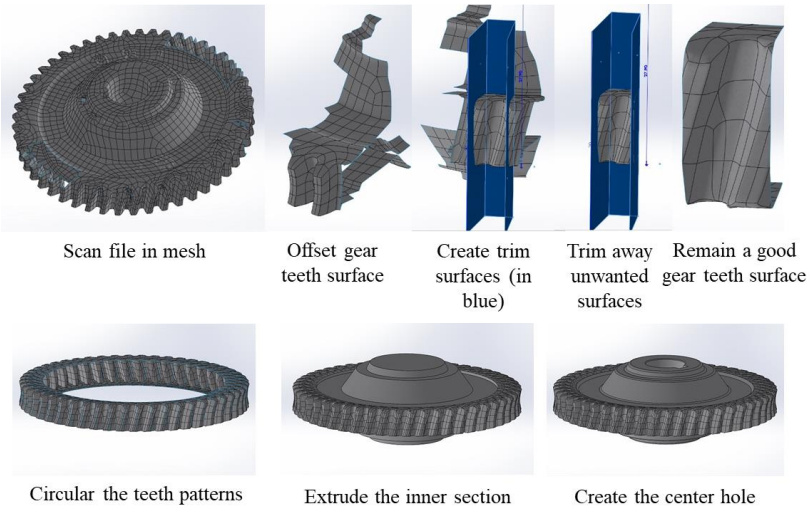

Fig. 15 3D surface reconstruction of the worm gear

In order to reveal the effect of tolerance of the polygon mesh body (STL format) on 3D printing parts, we varied the resolution setting before the CAD file of the worm gear being exported into STL format. Specifically, the deviation tolerance and angle tolerance were set as 0.0561mm and 10deg for the first printing, and 0.0501mm and 5deg for the second, as shown in Fig. 16.

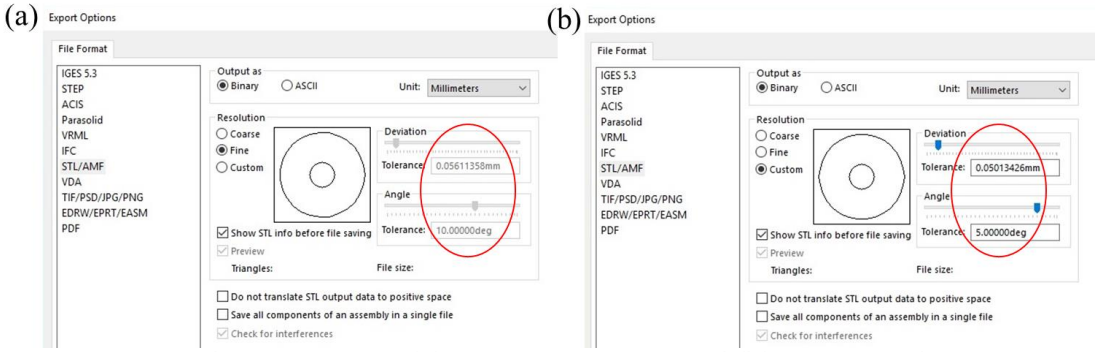

Fig. 16 Resolution setting: (a) for first printing and (b) for second printing

3D printing of the worm gear

The ABSplus-P430 and Nylon 12 worm gears were printed with the FDM technology on the 3D printers FDM uPrint SE plus and FDM Fortus 900MC, which took 2d 15h 52min and 23h 18min for printing 10 models, respectively. In comparison, the worm gear printed using PA 12 powder by MJF technology on MJF 4200/3200 took much shorter time, 2h 43min for printing 12 models, dramatically reducing the production costs. Meanwhile, PA 12 printing gear shows the better mechanical property, especially for its high elongation, which is discussed in Section 5.3.

As a better material selection, PA 12 for 3D printing worm gear was taken for analysis. The printing settings on MJF 4200/3200 are shown in Table 3. Fig. 17 shows the 3D printing worm gear in PA 12, and the cross section inspection indicates a high density, with no micro holes found inside the model.

Table 3 Printing settings of PA 12 worm gear

Mass of Worm Gears	840 g / 12 pcs
Processing Height	30.5 mm
Processing Time	2h 43m
Fusing Agent Usage	88 cc
Detailing Agent Usage	125.6 cc
Building Mode	Cosmetic

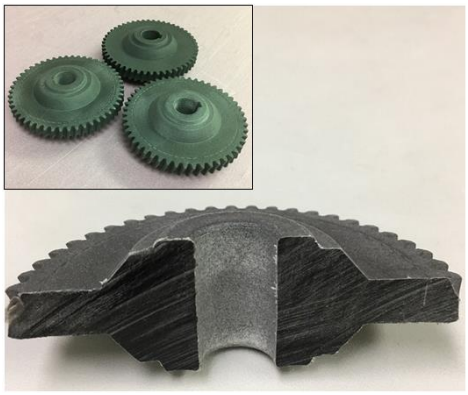

Fig. 17 3D printed worm gear of PA 12

Mechanical property evaluation of 3D printed worm gear

To obtain the tensile property of the worm gear, the Type V specimen was adopted according to the standard ASTM D638-10 and was cut from the original and 3D printing worm gears for tensile test. The geometry of the specimen is shown in Fig. 18. The tensile tests were conducted at room temperature by suing the tensile test instrument Instron Electropuls E10000 with a strain rate of 1.0×10^{-3}/s.

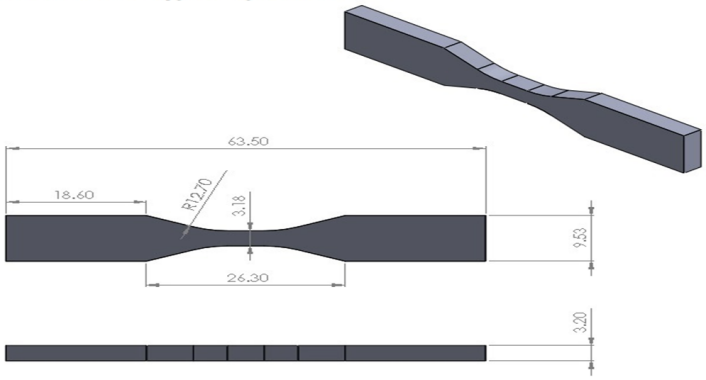

Fig. 18 ASTM D638-10 Type V specimen

Fig. 19 shows the engineering strain-stress curves of the original gear and the 3D printed gears using ABS, Nylon 12 (FDM) and PA 12 (MJF). The 3D printed worm gears all have higher elongation than the original one, although the latter indicates slightly higher tensile strength. Compared with Nylon 12 (FDM) and ABS, the specimen made of PA 12 (MJF) displays much better ductility with the fracture elongation of about 27%, much larger than the original one with 4.9%. As the worm gear made of PA 12 has the best plasticity, it could be a suitable material for making worm gear, which can undergo more deformation without damaging.

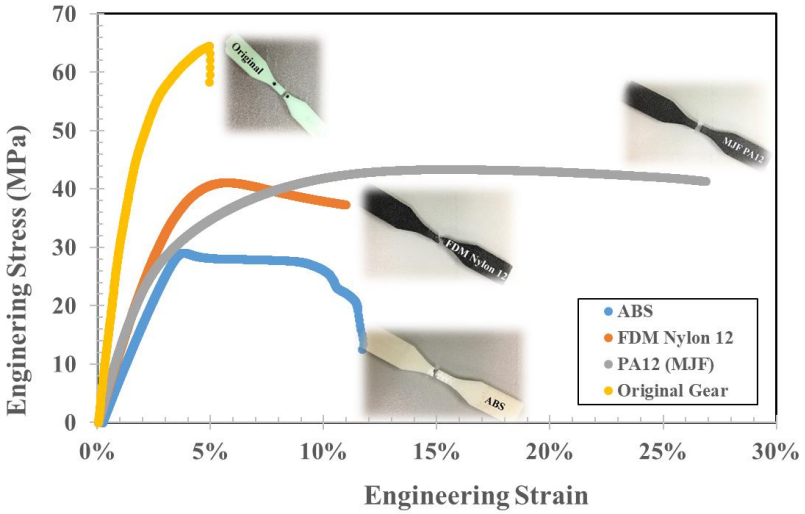

Fig. 19 Engineering strain-stress curves of the original gear and 3D printed gears using ABS, Nylon 12 (FDM) and PA 12 (MJF)

Geometry analysis of 3D printed worm gear

Fig. 20 illustrates the comparison of the Z-axis cross section inspection of PA 12 3D printing worm gears from STL files with two different resolution settings mentioned in Section 3.1. In the first printed sample (Fig. 20(a)), it shows that the addendum and dedendum of the printing sample is integrally lower than that of CAD body, with the maximum deviation reaching -0.09mm and -0.15mm, respectively.

However, in the second printed sample (Fig. 20(b)), a reasonable deviation is obtained, where the addendum of the printed sample is integrally higher than that of CAD body, the deviation maximumly reaching +0.05mm. The dedendum also has a much less deviation than that of the first sample, about -0.018mm in average.

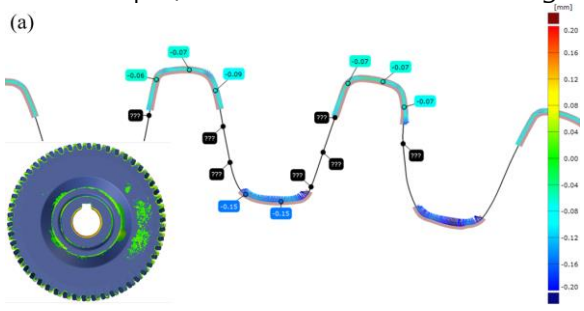

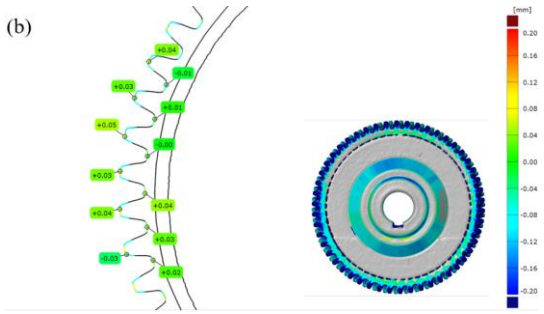

Fig. 20 Z-axis cross section inspection of worm gear:
(a) The first printed sample and (b) The second printed sample

In terms of inspections of the angle, radius/diameter and thickness, the second printed sample still shows a lower deviation than that of the first one, as shown in Fig. 21. Specially, the angle in the center of the gear has a maximum deviation of +9.53deg for the first printed sample, much larger than the second one (+0.00deg). And the radius/diameter and thickness inspections for both the first and second printed samples suggest an acceptable deviation.

Obviously, the precision of the second printed sample using the the STL file with the lower deviation and angle tolerance, would meet requirements better than the first printed sample.

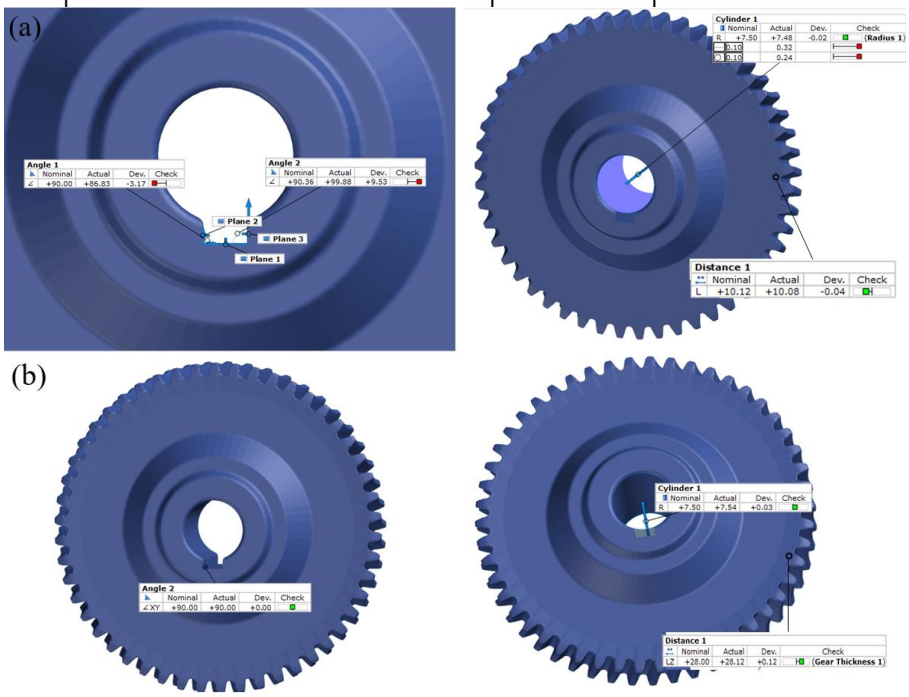

Fig. 21 Inspection of angle, radius/diameter and thickness of :
(a) The first printed sample and (b) the second printed sample

Conclusion and Way Forward

Conclusions

Based on RE technology, the 3D models of the critical parts in the shooting system were generated by potable 3D scanning system. The cube and worm gear were printed by using the dedicated 3D printers with different technologies and the selected materials. The evaluations of the mechanical properties and the forming accuracy of the 3D printed parts were conducted. The results can be summarized as follows:

(1) Stainless steel 316L powder was used to print the cube on the 3D printer SLM 280. The higher hardness was obtained compared to the original aluminum cube. The TF (top left) site on the substrate was found to have the higher fracture elongation than other sites for the printed cube.

(2) The forming quality of the 3D printer SLM 280 and WXL-120 used in printing the cube was compared. The specimen printed by the former shows a better surface quality and higher fracture elongation than that by the latter.

(3) Compared with Nylon 12 (FDM) and ABS (FDM), worm gear in PA 12 (MJF) has a shorter printing time (2h 43min for 12 models), and displays a much better ductility with the fracture elongation of 27%, much larger than the original one (4.9%).

(4) The geometry of 3D printing parts was verified compared with CAD model. The 3D printing cube was confirmed with a reasonable dimensional accuracy. For the 3D printed worm gear, a higher accuracy was obtained when we lowed the deviation and angle tolerance before exporting STL files.

To sum up, the cube and the worm gear fabricated by combing RE and 3D printing technology with the selected materials illustrate better performance than the original ones, thus can be well applied in the target shooting system.

Future Work

Fatigue test will be carried to evaluate the fatigue property of the 3D

printing parts from the selected materials. Besides, microstructure observations will be conducted to evaluate the microstructural characteristics and structural defects in the model.

For the selected materials, the corresponding 3D printing processes will be explored and further studied. The detailed process route, process window and the optimal process parameter configuration will be determined for the case study parts. The 3 to 4 case study parts will be rapidly manufactured by using the developed model and the 3D printing process, and the configured process parameters.

- END OF REPORT -

Digitalisation and Technology Division

Electrical and Mechanical Services Department

17 May 2019